

**Multicomponent dark matter systems and their observation prospects**Mayumi Aoki,<sup>1,2,\*</sup> Michael Duerr,<sup>2,†</sup> Jisuke Kubo,<sup>1,‡</sup> and Hiroshi Takano<sup>1,§</sup><sup>1</sup>*Institute for Theoretical Physics, Kanazawa University, Kanazawa 920-1192, Japan*<sup>2</sup>*Max-Planck-Institut für Kernphysik, Saupfercheckweg 1, 69117 Heidelberg, Germany*

(Received 19 July 2012; published 26 October 2012)

Conversions and semiannihilations of dark matter (DM) particles in addition to the standard DM annihilations are considered in a three-component DM system. We find that the relic abundance of DM can be very sensitive to these nonstandard DM annihilation processes, which has been recently found for two-component DM systems. To consider a concrete model of a three-component DM system, we extend the radiative seesaw model of Ma by adding a Majorana fermion  $\chi$  and a real scalar boson  $\phi$ , to obtain a  $Z_2 \times Z'_2$  DM stabilizing symmetry, where we assume that the DM particles are the inert Higgs boson,  $\chi$  and  $\phi$ . It is shown how the allowed parameter space, obtained previously in the absence of  $\chi$  and  $\phi$ , changes. The semiannihilation process in this model produces monochromatic neutrinos. The observation rate of these monochromatic neutrinos from the Sun at IceCube is estimated. Observations of high-energy monochromatic neutrinos from the Sun may indicate a multicomponent DM system.

DOI: [10.1103/PhysRevD.86.076015](https://doi.org/10.1103/PhysRevD.86.076015)

PACS numbers: 95.35.+d, 95.85.Ry, 11.30.Er

**I. INTRODUCTION**

Recent astrophysical observations [1–3] have made it clear that most of the energy of the Universe consists of dark energy and cold dark matter (DM), and their portions are very well fixed by these observations. While the origin of dark energy might be the cosmological constant of Einstein, the origin of cold DM cannot be found within the framework of the standard model (SM) of elementary particles. Moreover, we do not know very much about the detailed features of DM at present, even if the origin of DM should be elementary particles. Currently, many experiments are undertaken or planned, and it is widely believed that the existence of DM will be independently confirmed in the near future (see, for instance, Refs. [4–6]).

A particle DM candidate can be made stable by an unbroken symmetry. The simplest possibility of such a symmetry is a parity,  $Z_2$ . Whatever the origin of the  $Z_2$  is, the lightest  $Z_2$ -odd particle can be a DM candidate if it is a neutral, weakly interacting massive particle (see Ref. [5] for a review). There are a variety of origins of the  $Z_2$ .  $R$  parity in the minimal supersymmetric standard model, which is introduced to forbid fast proton decay, is a well-known example (see Ref. [4] for a review). In this paper, we consider a universe consisting of stable multi-DM particles [7–29]. A multicomponent DM system can be realized if the DM stabilizing symmetry is larger than  $Z_2$ :  $Z_N$  ( $N \geq 4$ ) or a product of two or more  $Z_2$ 's can yield a multicomponent DM system.<sup>1</sup> In a supersymmetric extension of the radiative seesaw model of Ref. [32], for

instance, a  $Z_2 \times Z'_2$  symmetry appears, providing various concrete models of multicomponent DM systems [25–29].

In a multicomponent DM system, there can be various DM annihilation processes that are different from the standard DM annihilation process [33–38],  $DM \rightarrow XX$ , where  $X$  is a generic SM particle in thermal equilibrium. Even in one-component DM systems, the nonstandard annihilation process, the coannihilation of DM and a nearly degenerate unstable particle [39], can play a crucial role in the minimal supersymmetric standard model [40]. The importance of nonstandard annihilation processes such as DM conversion [17,22,23] and semiannihilation of DM [17,23] in two-component DM systems for the temperature evolution of the number density of DM has been recently reported.

If  $(Z_2)^\ell$  is unbroken, there can exist at least  $K = \ell$  stable DM particles. In a kinematically fortunate situation,  $2^\ell - 1$  stable DM particles can exist; for  $\ell = 2$  there can be maximally  $K = 3$  stable DM particles. Any one-component DM model can easily be extended to a multicomponent DM system. The allowed parameter space of a one-component DM model can considerably change, as has been recently found in Ref. [29] (see also Ref. [10]), even using a crude approximation of a DM conversion process in a supersymmetric extension of the radiative seesaw model.

In Sec. II, after outlining a derivation of the coupled Boltzmann equations that are appropriate for our purpose, we consider fictive two- and three-component DM systems and analyze the effects of nonstandard annihilation processes of DM. In Sec. III, we extend the radiative seesaw model of Ref. [32] by adding an extra Majorana fermion  $\chi$  and an extra real scalar boson  $\phi$ , so as to obtain  $Z_2 \times Z'_2$  as a DM stabilizing symmetry. Apart from the presence of  $\phi$ , the Higgs sector is identical to that of Refs. [41–43]. This model shows how the allowed parameter space, which is obtained in Refs. [41–43] under the assumption that the

\*mayumi@hep.s.kanazawa-u.ac.jp

†michael.duerr@mpi-hd.mpg.de

‡jik@hep.s.kanazawa-u.ac.jp

§takano@hep.s.kanazawa-u.ac.jp

<sup>1</sup> $Z_3$  allows only one-component DM systems. Refs. [30,31] discuss models with  $Z_3$ .

lightest inert Higgs boson is DM, can change. Indirect detection of DM—in particular, of neutrinos from the annihilation of the captured DM in the Sun [44–53]—is also discussed. We solve the coupled evolution equations of the DM numbers in the Sun, which describe approaching equilibrium between the capture and annihilation (including conversion and semiannihilation) rates of DM, and estimate the observation rates of neutrinos. Due to semiannihilations of DM, monochromatic neutrinos are radiated from the Sun. Our conclusions are given in Sec. IV.

## II. THE BOLTZMANN EQUATION AND TWO- AND THREE-COMPONENT DM SYSTEMS

### A. The Boltzmann equation

Here we would like to outline a derivation of the Boltzmann equation that we are going to apply in the next section. We will do it for completeness, although the following discussion partially parallels that of Ref. [17] (see also Ref. [22]). We start by assuming the existence of  $K$  stable DM particles  $\chi_i$  with mass  $m_i$ . None of the DM particles have the same quantum number with respect to the DM stabilizing symmetry. All the other particles are supposed to be in thermal equilibrium. Then we restrict ourselves to three types of processes which enter the Boltzmann equation:

$$\chi_i \chi_i \leftrightarrow X_i X'_i, \quad (1)$$

$$\chi_i \chi_i \leftrightarrow \chi_j \chi_j \quad (\text{DM conversion}), \quad (2)$$

$$\chi_i \chi_j \leftrightarrow \chi_k X_{ijk} \quad (\text{DM semiannihilation}), \quad (3)$$

where the extension to include coannihilations and annihilation processes like  $\chi_i + \chi_j \leftrightarrow \chi_k + \chi_l$  is straightforward. See Fig. 1 for a depiction of DM conversion and DM semiannihilation.

We denote the phase space density of  $\chi_i$  by  $f_i(E_i, t)$  and its number density by  $n_i(t) = (g/(2\pi)^3) \int d^3 p_i f_i(E_i, t)$ , where  $g$  stands for the internal degrees of freedom. Then the density  $n_i$  satisfies the Boltzmann equation (see, e.g., Ref. [36]), which we will not spell out here. Instead, we make the replacement

$$t = 0.301 g_*^{-1/2} M_{\text{PL}} T^{-2}, \quad (4)$$

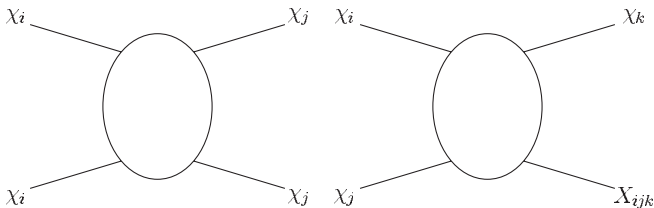


FIG. 1. Dark matter conversion (left) and semiannihilation (right).

during the radiation-dominated epoch, where  $t$  is the time of the comoving frame,  $g_*$  is the total number of effective degrees of freedom, and  $T$  and  $M_{\text{PL}}$  are the temperature and the Planck mass, respectively. Further, we use the approximation

$$\frac{f_i(E_i, t)}{\bar{f}_i(E_i, t)} \simeq \frac{n_i(t)}{\bar{n}_i(t)}, \quad (5)$$

where  $\bar{f}_i(E_i, t) \simeq \exp(-E_i/T)$  and  $\bar{n}_i = (g/(2\pi)^3) \times \int d^3 p_i \bar{f}_i(E_i, t)$  are the values in equilibrium, and we ignore the chemical potential. Then the collision terms in the Boltzmann equation can be written as

$$\begin{aligned} & - (\text{PSI}) |M(ii; X_i X'_i)|^2 \frac{\bar{f}_i \bar{f}_i}{\bar{n}_i \bar{n}_i} (n_i n_i - \bar{n}_i \bar{n}_i), \\ & - \sum_{i>j} (\text{PSI}) |M(ii; jj)|^2 \frac{\bar{f}_i \bar{f}_i}{\bar{n}_i \bar{n}_i} \left( n_i n_i - \frac{n_j n_j}{\bar{n}_j \bar{n}_j} \bar{n}_i \bar{n}_i \right), \\ & + \sum_{j>i} (\text{PSI}) |M(jj; ii)|^2 \frac{\bar{f}_j \bar{f}_j}{\bar{n}_j \bar{n}_j} \left( n_j n_j - \frac{n_i n_i}{\bar{n}_i \bar{n}_i} \bar{n}_j \bar{n}_j \right), \\ & - \sum_{j,k} (\text{PSI}) |M(ij; k X_{ijk})|^2 \frac{\bar{f}_i \bar{f}_j}{\bar{n}_i \bar{n}_j} \left( n_i n_j - \frac{n_k}{\bar{n}_k} \bar{n}_i \bar{n}_j \right), \\ & + \sum_{j,k} (\text{PSI}) |M(jk; i X_{jki})|^2 \frac{\bar{f}_j \bar{f}_k}{\bar{n}_j \bar{n}_k} \left( n_j n_k - \frac{n_i}{\bar{n}_i} \bar{n}_j \bar{n}_k \right), \end{aligned} \quad (6)$$

where PSI stands for “phase space integral of  $(2\pi)^4 \delta^4(\text{momenta}) \times$ ,”  $M$  is the matrix element of the corresponding process, and we have assumed that

$$m_i \geq m_j \quad \text{for } i > j \quad \text{and} \quad m_{X_i}, m_{X'_i}, m_{X_{ijk}} \ll m_i \quad \text{for all } i, j, k, l. \quad (7)$$

Using the notion of the thermally averaged cross section,

$$\langle \sigma(ii; X_i X'_i) v \rangle = \frac{1}{\bar{n}_i \bar{n}_i} \text{PSI} |M(ii; X_i X'_i)|^2 \bar{f}_i \bar{f}_i, \quad (8)$$

and the dimensionless inverse temperature  $x = \mu/T$ , we obtain for the number per comoving volume,  $Y_i = n_i/s$ :

$$\begin{aligned} \frac{dY_i}{dx} = & -0.264 g_*^{1/2} \left[ \frac{\mu M_{\text{PL}}}{x^2} \right] \left\{ \langle \sigma(ii; X_i X'_i) v \rangle (Y_i Y_i - \bar{Y}_i \bar{Y}_i) \right. \\ & + \sum_{i>j} \langle \sigma(ii; jj) v \rangle \left( Y_i Y_i - \frac{Y_j Y_j}{\bar{Y}_j \bar{Y}_j} \bar{Y}_i \bar{Y}_i \right) \\ & - \sum_{j>i} \langle \sigma(jj; ii) v \rangle \left( Y_j Y_j - \frac{Y_i Y_i}{\bar{Y}_i \bar{Y}_i} \bar{Y}_j \bar{Y}_j \right) \\ & + \sum_{j,k} \langle \sigma(ij; k X_{ijk}) v \rangle \left( Y_i Y_j - \frac{Y_k}{\bar{Y}_k} \bar{Y}_i \bar{Y}_j \right) \\ & \left. - \sum_{j,k} \langle \sigma(jk; i X_{jki}) v \rangle \left( Y_j Y_k - \frac{Y_i}{\bar{Y}_i} \bar{Y}_j \bar{Y}_k \right) \right\}, \end{aligned} \quad (9)$$

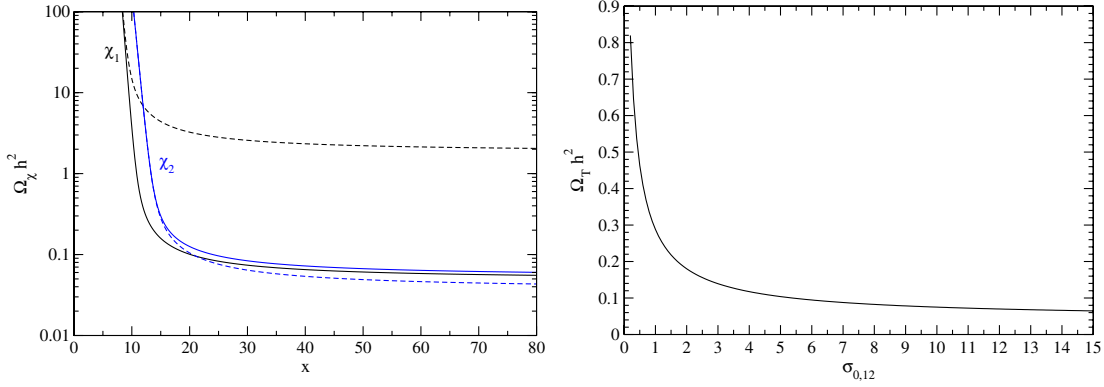


FIG. 2 (color online). Left: The relic abundance  $\Omega_{\chi_1} h^2(x)$  (black curves) and  $\Omega_{\chi_2} h^2(x)$  (blue curves) as a function of  $x = \mu/T = [(m_1^{-1} + m_2^{-1})T]^{-1}$ , with  $\sigma_{0,1} = 0.1$ ,  $\sigma_{0,2} = 6$ ,  $\sigma_{0,12} = 4.4$  (solid curves) or 0 (dashed curves),  $m_1 = 200$  GeV,  $m_2 = 160$  GeV, and  $g_* = 90$ . Right: The total relic abundance  $\Omega_T h^2$  as a function of  $\sigma_{0,12}$ , which parametrizes the size of the conversion  $\chi_1 \chi_1 \rightarrow \chi_2 \chi_2$ .

where  $1/\mu = (\sum_i m_i^{-1})$  is the reduced mass of the system. To arrive at Eq. (9), we have used  $s = (2\pi^2/45)g_*T^3$ ,  $H = 1.66 \times g_*^{1/2}T^2/M_{\text{PL}}$ , where  $s$  is the entropy density and  $H$  is the Hubble constant.

We will integrate this system of coupled nonlinear differential equations numerically. Before we apply the Boltzmann equation [Eq. (9)] to a concrete DM model, we discuss below the cases of  $K = 2$  and 3, simply assuming fictitious values of the thermally averaged cross sections and DM masses  $m_i$ .

### B. Two-component DM system

Before we come to one of our main interests, a three-component DM system, we first consider the  $K = 2$  case with a  $Z_2 \times Z'_2$  symmetry. In this case, there are three different thermally averaged cross sections. No semiannihilation [Eq. (3)] is allowed due to  $Z_2 \times Z'_2$ .<sup>2</sup> We further assume that there are only  $s$ -wave contributions to  $\langle\sigma v\rangle$  and that  $X_i (i = 1, 2)$  are massless while  $m_1 \geq m_2$ :

$$\begin{aligned} \langle\sigma(11; X_1 X'_1)v\rangle &= \sigma_{0,1} \times 10^{-9} \text{ GeV}^{-2}, \\ \langle\sigma(22; X_2 X'_2)v\rangle &= \sigma_{0,2} \times 10^{-9} \text{ GeV}^{-2}, \\ \langle\sigma(11; 22)v\rangle &= \sigma_{0,12} \times 10^{-9} \text{ GeV}^{-2}. \end{aligned} \quad (10)$$

Equation (9) then becomes

$$\begin{aligned} \frac{dY_1}{dx} &= -0.264g_*^{1/2} \left[ \frac{\mu M_{\text{PL}}}{x^2} \right] \left\{ \langle\sigma(11; X_1 X'_1)v\rangle (Y_1 Y_1 - \bar{Y}_1 \bar{Y}_1) \right. \\ &\quad \left. + \langle\sigma(11; 22)v\rangle \left( Y_1 Y_1 - \frac{Y_2 Y_2}{\bar{Y}_2 \bar{Y}_2} \bar{Y}_1 \bar{Y}_1 \right) \right\}, \end{aligned} \quad (11)$$

<sup>2</sup>In Refs. [17,23], the  $Z_4$  case is discussed in detail. In this case there exist two independent DM particles, because due to  $CP$  invariance, the antiparticle is not an independent degree of freedom in the Boltzmann equation. Semiannihilation is allowed in this case.

$$\begin{aligned} \frac{dY_2}{dx} &= -0.264g_*^{1/2} \left[ \frac{\mu M_{\text{PL}}}{x^2} \right] \left\{ \langle\sigma(22; X_2 X'_2)v\rangle (Y_2 Y_2 - \bar{Y}_2 \bar{Y}_2) \right. \\ &\quad \left. - \langle\sigma(11; 22)v\rangle \left( Y_1 Y_1 - \frac{Y_2 Y_2}{\bar{Y}_2 \bar{Y}_2} \bar{Y}_1 \bar{Y}_1 \right) \right\}. \end{aligned} \quad (12)$$

We consider the case in which the sizes of the DM conversion and the standard annihilation are of similar order (see also Ref. [22]). In Fig. 2 (left), we show the evolution of the fraction of critical densities,  $\Omega_{\chi_1} h^2(x)$  (black curves) and  $\Omega_{\chi_2} h^2(x)$  (blue curves), contributed by  $\chi_1$  and  $\chi_2$ , respectively, where we have used  $\sigma_{0,1} = 0.1$ ,  $\sigma_{0,2} = 6$ ,  $\sigma_{0,12} = 4.4$  (solid curves) or 0 (dashed curves),  $m_1 = 200$  GeV,  $m_2 = 160$  GeV,  $g_* = 90$ , and  $x = \mu/T = [(m_1^{-1} + m_2^{-1})T]^{-1}$ . As we see from Fig. 2 (left), at  $\sigma_{0,12} = 0$  [i.e., no DM conversion, Eq. (2)], the density of  $\chi_1$  decouples from the equilibrium value for smaller  $x$  than the density of  $\chi_2$  does. This is because we have chosen a small value for  $\sigma_{0,1}$  and a large value for  $\sigma_{0,2}$ . At  $\sigma_{0,12} = 0$ ,  $\Omega_{\chi_1} h^2 \approx 1.99$ , while  $\Omega_{\chi_2} h^2 \approx 0.04$ . With increasing values of  $\sigma_{0,12}$  [which parametrizes the size of the DM conversion, Eq. (2)],  $\Omega_{\chi_1} h^2$  decreases, while  $\Omega_{\chi_2} h^2$  increases. Around  $\sigma_{0,12} = 3.9$ , this order changes, i.e.,  $\Omega_{\chi_1} < \Omega_{\chi_2}$ . At  $\sigma_{0,12} = 4.4$ , we obtain the total relic abundance  $\Omega_T h^2 = \Omega_{\chi_1} h^2 + \Omega_{\chi_2} h^2 = 0.112$ , in accord with the WMAP observation  $\Omega_T h^2 = 0.1126 \pm 0.0036$  [3]. In Fig. 2 (right), we plot  $\Omega_T h^2$  as a function of  $\sigma_{0,12}$ . We see that the DM conversion process plays an important role, as has also been found in Refs. [12,17,22,23].

### C. Three-component DM system

As we have noticed before, the  $K = 3$  case is possible even for a  $Z_2 \times Z'_2$  symmetry if the decay of  $\chi_i$  is kinematically forbidden. In this case, there are nine different thermally averaged cross sections, if we assume that  $m_1 \geq m_2 \geq m_3$  and  $m_2 + m_3 > m_1$ :

$$\begin{aligned}
\langle\sigma(ii; X_i X'_i)v\rangle &= \sigma_{0,i} \times 10^{-9} \text{ GeV}^{-2}, & \langle\sigma(11; 22)v\rangle &= \sigma_{0,12} \times 10^{-9} \text{ GeV}^{-2}, \\
\langle\sigma(11; 33)v\rangle &= \sigma_{0,13} \times 10^{-9} \text{ GeV}^{-2}, & \langle\sigma(22; 33)v\rangle &= \sigma_{0,23} \times 10^{-9} \text{ GeV}^{-2}, \\
\langle\sigma(12; 3X_{123})v\rangle &= \sigma_{0,123} \times 10^{-9} \text{ GeV}^{-2}, & \langle\sigma(23; 1X_{231})v\rangle &= \sigma_{0,231} \times 10^{-9} \text{ GeV}^{-2}, \\
\langle\sigma(31; 2X_{312})v\rangle &= \sigma_{0,312} \times 10^{-9} \text{ GeV}^{-2}.
\end{aligned} \tag{13}$$

Equation (9) then becomes

$$\begin{aligned}
\frac{dY_1}{dx} &= -0.264g_*^{1/2} \left[ \frac{\mu M_{\text{PL}}}{x^2} \right] \left\{ \langle\sigma(11; X_1 X'_1)v\rangle (Y_1 Y_1 - \bar{Y}_1 \bar{Y}_1) + \langle\sigma(11; 22)v\rangle \left( Y_1 Y_1 - \frac{Y_2 Y_2}{\bar{Y}_2 \bar{Y}_2} \bar{Y}_1 \bar{Y}_1 \right) \right. \\
&+ \langle\sigma(11; 33)v\rangle \left( Y_1 Y_1 - \frac{Y_3 Y_3}{\bar{Y}_3 \bar{Y}_3} \bar{Y}_1 \bar{Y}_1 \right) + \langle\sigma(12; 3X_{123})v\rangle \left( Y_1 Y_2 - \frac{Y_3}{\bar{Y}_3} \bar{Y}_1 \bar{Y}_2 \right) + \langle\sigma(31; 2X_{312})v\rangle \left( Y_1 Y_3 - \frac{Y_2}{\bar{Y}_2} \bar{Y}_1 \bar{Y}_3 \right) \\
&\left. - \langle\sigma(23; 1X_{231})v\rangle \left( Y_3 Y_2 - \frac{Y_1}{\bar{Y}_1} \bar{Y}_3 \bar{Y}_2 \right) \right\}, \tag{14}
\end{aligned}$$

$$\begin{aligned}
\frac{dY_2}{dx} &= -0.264g_*^{1/2} \left[ \frac{\mu M_{\text{PL}}}{x^2} \right] \left\{ \langle\sigma(22; X_2 X'_2)v\rangle (Y_2 Y_2 - \bar{Y}_2 \bar{Y}_2) + \langle\sigma(22; 33)v\rangle \left( Y_2 Y_2 - \frac{Y_3 Y_3}{\bar{Y}_3 \bar{Y}_3} \bar{Y}_2 \bar{Y}_2 \right) \right. \\
&+ \langle\sigma(23; 1X_{231})v\rangle \left( Y_2 Y_3 - \frac{Y_1}{\bar{Y}_1} \bar{Y}_2 \bar{Y}_3 \right) + \langle\sigma(12; 3X_{123})v\rangle \left( Y_1 Y_2 - \frac{Y_3}{\bar{Y}_3} \bar{Y}_1 \bar{Y}_2 \right) - \langle\sigma(31; 2X_{312})v\rangle \left( Y_1 Y_3 - \frac{Y_2}{\bar{Y}_2} \bar{Y}_1 \bar{Y}_3 \right) \\
&\left. - \langle\sigma(11; 22)v\rangle \left( Y_1 Y_1 - \frac{Y_2 Y_2}{\bar{Y}_2 \bar{Y}_2} \bar{Y}_1 \bar{Y}_1 \right) \right\}, \tag{15}
\end{aligned}$$

$$\begin{aligned}
\frac{dY_3}{dx} &= -0.264g_*^{1/2} \left[ \frac{\mu M_{\text{PL}}}{x^2} \right] \left\{ \langle\sigma(33; X_3 X'_3)v\rangle (Y_3 Y_3 - \bar{Y}_3 \bar{Y}_3) + \langle\sigma(23; 1X_{231})v\rangle \left( Y_2 Y_3 - \frac{Y_1}{\bar{Y}_1} \bar{Y}_2 \bar{Y}_3 \right) \right. \\
&+ \langle\sigma(31; 2X_{312})v\rangle \left( Y_1 Y_3 - \frac{Y_2}{\bar{Y}_2} \bar{Y}_1 \bar{Y}_3 \right) - \langle\sigma(12; 3X_{123})v\rangle \left( Y_1 Y_2 - \frac{Y_3}{\bar{Y}_3} \bar{Y}_1 \bar{Y}_2 \right) - \langle\sigma(11; 33)v\rangle \left( Y_1 Y_1 - \frac{Y_3 Y_3}{\bar{Y}_3 \bar{Y}_3} \bar{Y}_1 \bar{Y}_1 \right) \\
&\left. - \langle\sigma(22; 33)v\rangle \left( Y_2 Y_2 - \frac{Y_3 Y_3}{\bar{Y}_3 \bar{Y}_3} \bar{Y}_2 \bar{Y}_2 \right) \right\}, \tag{16}
\end{aligned}$$

where  $1/\mu = 1/m_1 + 1/m_2 + 1/m_3$ .

As a representative example, we consider the following set of input values of the parameters:

$$\begin{aligned}
m_1 &= 200 \text{ GeV}, & m_2 &= 160 \text{ GeV}, & m_3 &= 140 \text{ GeV}, \\
\sigma_{0,1} &= 0.1, & \sigma_{0,2} &= 2, & \sigma_{0,3} &= 6.
\end{aligned} \tag{17}$$

First, we show the evolution of  $\Omega_{\chi_i} h^2(x)$  in Fig. 3 (left) for  $\sigma_{0,12} = \sigma_{0,13} = \sigma_{0,23} = \sigma_{0,123} = \sigma_{0,312} = \sigma_{0,231} = 0$ , which corresponds to the situation without the nonstandard annihilation processes. Since  $m_1 > m_2, m_3$ , and the cross section  $\sigma(11; X_1 X_1)$  is small in this example, the relic abundance of  $\chi_1$  is large compared with that of  $\chi_2$  and  $\chi_3$ . This changes if we switch on the nonstandard annihilation processes. This is shown in Fig. 3 (right), where we have used  $\sigma_{0,12} = \sigma_{0,13} = \sigma_{0,23} = 5.2$ , while  $\sigma_{0,123} = \sigma_{0,312} = \sigma_{0,231} = 0$ , to show the effects of  $\chi_i \chi_i \leftrightarrow \chi_j \chi_j$ -type processes (DM conversion). As expected, the relic abundances of  $\chi_1$  and  $\chi_2$  decrease and drop below 0.1, while that of  $\chi_3$  does not change very much.

Figure 4 shows the evolution of  $\Omega_{\chi_i} h^2(x)$  for  $\sigma_{0,12} = \sigma_{0,13} = \sigma_{0,23} = 0$ , while  $\sigma_{0,123} = \sigma_{0,312} = \sigma_{0,231} = 5.1$ ,

to show the effects of  $\chi_i \chi_j \leftrightarrow \chi_k X_{ijk}$ -type processes (semiannihilation). It is interesting to observe that the order of the relic abundances changes, and  $\Omega_{\chi_1} h^2(x)$  first decreases as usual, but then starts to increase towards the freeze-out value. So, the effects of  $\chi_i \chi_i \leftrightarrow \chi_j \chi_j$ -type and  $\chi_i \chi_j \leftrightarrow \chi_k X_{ijk}$ -type processes are different. In the examples above,  $\sigma_{0,ij}$  and  $\sigma_{0,ijk}$  are chosen such that the total abundance  $\Omega_T h^2$  becomes about the realistic value 0.112. In Fig. 5, we show the total abundance  $\Omega_T h^2$  as a function of  $\sigma_{0,ij}$  (solid curve) and  $\sigma_{0,ijk}$  (dashed curve), where  $\sigma_{0,ij}$  parameterizes the size of the DM conversion [Eq. (2)] and  $\sigma_{0,ijk}$  parameterizes the size of the semiannihilation [Eq. (3)]. As we can see from Fig. 5, only for small values of  $\sigma_{0,ij}$  and  $\sigma_{0,ijk}$  are the effects on  $\Omega_T h^2$  different.

Note that the dark matter conversion process [Eq. (2)] is dark-matter-number conserving, while the semiannihilation process [Eq. (3)] is not. Next, we would like to consider an extreme case where only semiannihilations are present, and as before we assume that  $m_1 \geq m_2 \geq m_3$  and  $m_2 + m_3 > m_1$ . In Table I, we show various examples of the individual relic abundances with  $m_1$  fixed at 1000 GeV,

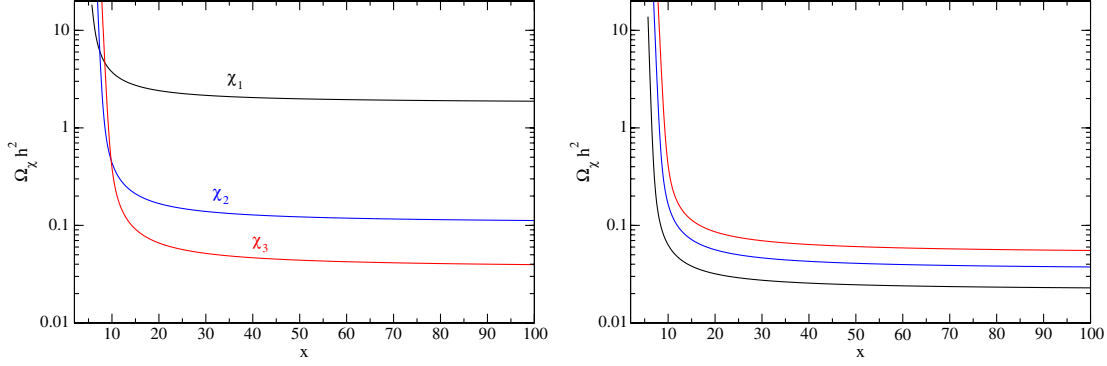


FIG. 3 (color online). The relic abundance  $\Omega_{\chi_1} h^2(x)$  (black curve),  $\Omega_{\chi_2} h^2(x)$  (blue curve) and  $\Omega_{\chi_3} h^2(x)$  (red curve) as a function of  $x = \mu/T = [(m_1^{-1} + m_2^{-1} + m_3^{-1})T]^{-1}$ , where the input parameters are given in Eq. (17). Left: Without the nonstandard annihilation processes [Eqs. (2) and (3)]. Right:  $\sigma_{0,12} = \sigma_{0,13} = \sigma_{0,23} = 5.2$ , while  $\sigma_{0,123} = \sigma_{0,312} = \sigma_{0,231} = 0$ , to show the effects of  $\chi_i \chi_i \leftrightarrow \chi_j \chi_j$ -type processes [Eq. (3)].

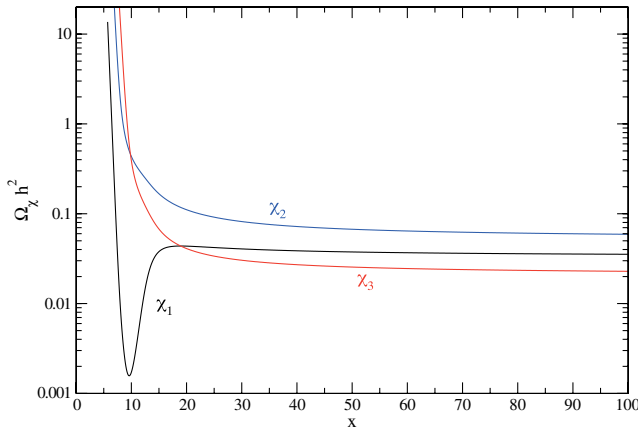


FIG. 4 (color online). The relic abundance  $\Omega_{\chi_1} h^2(x)$  (black curve),  $\Omega_{\chi_2} h^2(x)$  (blue curve) and  $\Omega_{\chi_3} h^2(x)$  (red curve) as a function of  $x$  with  $\sigma_{0,12} = \sigma_{0,13} = \sigma_{0,23} = 0$ , while  $\sigma_{0,123} = \sigma_{0,312} = \sigma_{0,231} = 5.1$ , to show the effects of  $\chi_i \chi_j \leftrightarrow \chi_k X_{ijk}$ -type processes [Eq. (3)].

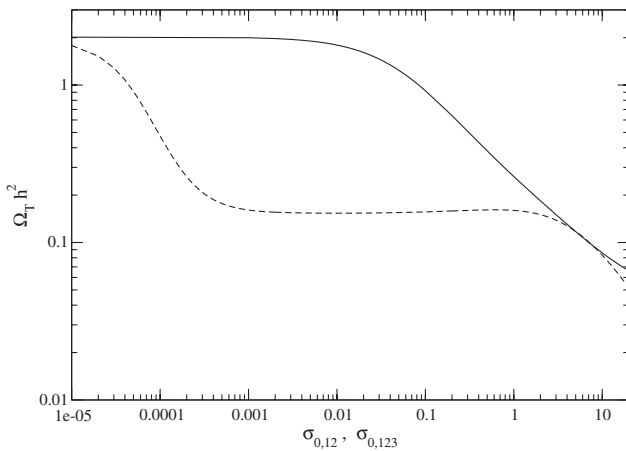


FIG. 5. The total relic abundance  $\Omega_T h^2$  as a function of  $\sigma_{0,12}$  (solid curve) and  $\sigma_{0,123}$  (dashed curve). Except for  $\sigma_{0,12}$  (DM conversion) and  $\sigma_{0,123}$  (semiannihilation), the input parameters are as given in Eq. (17).

where we have assumed that the value of  $\sigma_{0,ijk}$  is the same independent of  $i, j$  and  $k$ . These values are chosen such that the total relic abundance is consistent with  $\Omega_T h^2 = 0.1126 \pm 0.0036$ . As we see from Table I, depending on the hierarchy of the dark matter masses, the value of  $\sigma_{0,123}$  has to be tuned to obtain the observed value of the total relic abundance. We may say that the more hierarchical the dark matter masses are, the larger  $\sigma_{0,123}$  is, and the larger  $\Omega_{\chi_3} h^2$  is. We then consider the asymmetric case, i.e.,  $\sigma_{0,123} \neq \sigma_{0,231} \neq \sigma_{0,312}$ . In Table II, we give some examples of this case with fixed dark matter masses,  $m_1 = 1000$  GeV,  $m_2 = 900$  GeV and  $m_3 = 550$  GeV, where we have assumed that  $m_1$  and  $m_2$  are close, but  $m_3$  is about one half of  $m_1$ . Since  $\sigma_{0,123}$  is the size for the semiannihilation  $\chi_1 \chi_2 \rightarrow \chi_3 X$ , the relic abundance of  $\chi_3$  is larger than the others for larger  $\sigma_{0,123}$ . Finally, we would like to point out that, since each semiannihilation produces

TABLE I. The relic abundances for the symmetric case of  $\sigma_{0,ijk}$ ; i.e.,  $\sigma_{0,123} = \sigma_{0,231} = \sigma_{0,312}$ , with  $m_1 = 1000$  GeV.

$m_2$	$m_3$	$\sigma_{0,123}$	$\Omega_{\chi_1} h^2$	$\Omega_{\chi_2} h^2$	$\Omega_{\chi_3} h^2$
720	700	12.6	0.0433	0.0319	0.0372
940	700	417.0	0.0007	0.0007	0.1109
600	550	42.3	0.0431	0.0259	0.0439
840	550	7900	0.0001	0.0001	0.1117

TABLE II. The relic abundances for the asymmetric case; i.e.,  $\sigma_{0,123} \neq \sigma_{0,231} \neq \sigma_{0,312}$ , with  $m_1 = 1000$  GeV,  $m_2 = 900$  GeV and  $m_3 = 550$  GeV.

$\sigma_{0,123}$	$\sigma_{0,231}$	$\sigma_{0,312}$	$\Omega_{\chi_1} h^2$	$\Omega_{\chi_2} h^2$	$\Omega_{\chi_3} h^2$
48.0	2000.0	48.4	0.0325	0.0007	0.0793
55.5	65.0	2000.0	0.0003	0.1118	0.0002
90.0	1000.0	100.3	0.0121	0.0011	0.0988
110.0	600.0	145.2	0.0067	0.0015	0.1039

a DM particle, the semiannihilation process can be a few orders of magnitude larger than the standard process where only the standard process exists (as we can see from Tables I and II). The magnitude, of course, depends on a model, but this can be useful information for model building.

### III. A MODEL WITH THREE DARK MATTER PARTICLES

We extend the original radiative seesaw model of Ref. [32] so as to have an additional discrete symmetry,  $Z'_2$ . This can be done by introducing a SM singlet Majorana fermion  $\chi$  and a SM singlet real inert scalar  $\phi$  in addition to the inert Higgs doublet  $\eta$  which is present in the original model. The matter content of the model with the corresponding quantum numbers is given in Table III.

The  $Z_2 \times Z'_2$ -invariant Yukawa couplings of the lepton sector are given by

$$\mathcal{L}_Y = Y_{ij}^e H^\dagger L_i l_j^c + Y_{ik}^\nu L_i \epsilon \eta N_k^c + Y_k^\chi \chi N_k^c \phi + \text{H.c.}, \quad (18)$$

and the Majorana mass terms of the right-handed neutrinos  $N_k^c$  ( $k = 1, 2, 3$ ) and the singlet fermion  $\chi$  are<sup>3</sup>

$$\mathcal{L}_{\text{Maj}} = \frac{1}{2} M_k N_k^c N_k^c + \frac{1}{2} M_\chi \chi^2 + \text{H.c.} \quad (19)$$

We may assume without loss of generality that the right-handed neutrino mass matrix is diagonal and real. As far as the light neutrino masses, which are generated radiatively, are concerned, the last additional interaction term in Eq. (18) has no influence. So the neutrino phenomenology is the same as in the original model. The most general form of the  $Z_2 \times Z'_2$ -invariant scalar potential can be written as

$$\begin{aligned} V = & m_1^2 H^\dagger H + m_2^2 \eta^\dagger \eta + \frac{1}{2} m_3^2 \phi^2 + \frac{1}{2} \lambda_1 (H^\dagger H)^2 \\ & + \frac{1}{2} \lambda_2 (\eta^\dagger \eta)^2 + \lambda_3 (H^\dagger H)(\eta^\dagger \eta) + \lambda_4 (H^\dagger \eta)(\eta^\dagger H) \\ & + \frac{1}{2} \lambda_5 [(H^\dagger \eta)^2 + \text{H.c.}] + \frac{1}{4!} \lambda_6 \phi^4 + \frac{1}{2} \lambda_7 (H^\dagger H) \phi^2 \\ & + \frac{1}{2} \lambda_8 (\eta^\dagger \eta) \phi^2, \end{aligned} \quad (20)$$

from which we obtain the masses of the inert Higgs fields:

$$m_{\eta^\pm}^2 = m_2^2 + \lambda_3 v^2/2, \quad (21)$$

$$m_{\eta_R}^2 = m_2^2 + (\lambda_3 + \lambda_4 + \lambda_5) v^2/2 = m_2^2 + \lambda_L v^2/2, \quad (22)$$

$$m_{\eta_I}^2 = m_2^2 + (\lambda_3 + \lambda_4 - \lambda_5) v^2/2, \quad (23)$$

$$m_\phi^2 = m_3^2 + \lambda_7 v^2/2. \quad (24)$$

<sup>3</sup>A similar model is considered in Ref. [12].

TABLE III. The matter content of the model and the corresponding quantum numbers.  $Z_2 \times Z'_2$  is the unbroken discrete symmetry. The quarks are suppressed in the table.

Field	$SU(2)_L$	$U(1)_Y$	$Z_2$	$Z'_2$
$(\nu_{Li}, l_i)$	2	-1/2	+	+
$l_i^c$	1	1	+	+
$N_i^c$	1	0	-	+
$H = (H^+, H^0)$	2	1/2	+	+
$\eta = (\eta^+, \eta^0)$	2	1/2	-	+
$\chi$	1	0	+	-
$\phi$	1	0	-	-

Here,  $\langle H \rangle = v/\sqrt{2}$  is the Higgs vacuum expectation value, and  $\eta^0 = (\eta_R^0 + i\eta_I^0)/\sqrt{2}$ . At this stage, we have assumed that

$$\langle H \rangle = v/\sqrt{2}, \quad \langle \eta \rangle = \langle \phi \rangle = 0, \quad (25)$$

correspond to the absolute minimum. [The sufficient condition for the absolute minimum of Eq. (20) is given below.] As we can see from Table III, the cold DM candidates are  $N_k^c$ ,  $\eta_R^0$ ,  $\eta_I^0$ ,  $\chi$  and  $\phi$ , where  $\eta_R^0$  as dark matter in the original model has been discussed in detail in Refs. [41–43]. To proceed, we assume that the mass relations

$$\begin{aligned} M_k \gg m_{\eta^\pm}, m_{\eta_I^0} > m_{\eta_R^0} > m_\phi, m_\chi \quad \text{and} \\ m_{\eta_R^0} < m_\phi + m_\chi, \end{aligned} \quad (26)$$

are satisfied.<sup>4</sup> These relations are chosen because we would like to meet the following requirements:

(1)  $\mu \rightarrow e\gamma$ .

The constraint coming from  $\mu \rightarrow e\gamma$  is given by [54]

$$\begin{aligned} B(\mu \rightarrow e\gamma) &= \frac{3\alpha}{64\pi(G_F m_{\eta^\pm}^2)^2} \left| \sum_k Y_{\mu k}^\nu Y_{ek}^\nu F_2 \left( \frac{M_k^2}{m_{\eta^\pm}^2} \right) \right|^2 \\ &\leq 2.4 \times 10^{-12}, \end{aligned}$$

$$F_2(x) = \frac{1}{6(1-x)^4} (1 - 6x + 3x^2 + 2x^3 - 6x^2 \ln x), \quad (27)$$

where the upper bound is taken from Ref. [55]. A similar, but slightly weaker bound for  $\tau \rightarrow \mu(e)\gamma$  given in Ref. [55] has to be satisfied, too. Since  $F_2(x) \sim 1/3x$  for  $x \gg 1$ , while  $1/12 < F_2(x) < 1/6$  for  $0 < x < 1$ , the constraint can be readily satisfied if  $M_k \ll m_{\eta^\pm}$  or  $M_k \gg m_{\eta^\pm}$ .

<sup>4</sup>The possibility  $m_{\eta_I^0} < m_{\eta_R^0}$  does not give any new feature of the model.

(2)  $g_\mu - 2$ .

The extra contribution to the anomalous magnetic moment of the muon,  $a_\mu = (g_\mu - 2)/2$ , is given by [54]

$$\delta a_\mu = \frac{m_\mu^2}{16\pi^2 m_{\eta^\pm}^2} \sum_k Y_{\mu k}^\nu Y_{\mu k}^\nu F_2\left(\frac{M_k^2}{m_{\eta^\pm}^2}\right). \quad (28)$$

If we assume that  $|\sum_k Y_{\mu k}^\nu Y_{\mu k}^\nu F_2(\frac{M_k^2}{m_{\eta^\pm}^2})| \simeq |\sum_k Y_{\mu k}^\nu Y_{e k}^\nu F_2(\frac{M_k^2}{m_{\eta^\pm}^2})|$ , then we obtain

$$|\delta a_\mu| \simeq 2.2 \times 10^{-5} B(\mu \rightarrow e\gamma) \lesssim 3.4 \times 10^{-11}, \quad (29)$$

if Eq. (27) is satisfied, where the upper bound is taken from Ref. [56]. So, the constraint from  $a_\mu$  has no significant influence.

(3) Stable and global minimum.

The DM stabilizing symmetry  $Z_2$  remains unbroken if

$$m_1^2 < 0, \quad m_2^2 > 0, \quad m_3^2 > 0,$$

$$\lambda_1, \lambda_2, \lambda_6 > 0, \quad \lambda_3 + \lambda_4 - |\lambda_5|, \quad \lambda_3 > -\frac{1}{2}(\lambda_1 \lambda_2)^{1/2},$$

$$\lambda_7 > -\frac{1}{2}(\lambda_1 \lambda_6/3)^{1/2}, \quad \lambda_8 > -\frac{1}{2}(\lambda_2 \lambda_6/3)^{1/2}, \quad (30)$$

are satisfied. These conditions are sufficient for Eq. (25) to correspond to the absolute minimum. Since  $m_{\eta_R}^2 - m_{\eta_I}^2 = \lambda_5 v^2$ , a negative  $\lambda_5$  is consistent with Eq. (26).

(4) Electroweak precision.

The electroweak precision measurement requires [41,56]

$$\begin{aligned} \Delta T &\simeq 0.54 \left( \frac{m_{\eta^\pm} - m_{\eta_R}^0}{v} \right) \left( \frac{m_{\eta^\pm} - m_{\eta_I}^0}{v} \right) \\ &= 0.02_{-0.12}^{+0.11}, \end{aligned} \quad (31)$$

for  $m_h = 115\text{--}127$  GeV. Therefore,  $|m_{\eta^\pm} - m_{\eta_R}^0|$ ,  $|m_{\eta^\pm} - m_{\eta_I}^0| \lesssim 100$  GeV is sufficient to meet the requirement.

Then, with the assumption of the above mass relations, we look at the radiative neutrino mass matrix [32]:

$$\begin{aligned} (\mathcal{M}_\nu)_{ij} &= \sum_k \frac{Y_{ik}^\nu Y_{jk}^\nu M_k}{16\pi^2} \left[ \frac{m_{\eta_R}^2}{m_{\eta_R}^2 - M_k^2} \ln\left(\frac{m_{\eta_R}^0}{M_k}\right)^2 \right. \\ &\quad \left. - \frac{m_{\eta_I}^2}{m_{\eta_I}^2 - M_k^2} \ln\left(\frac{m_{\eta_I}^0}{M_k}\right)^2 \right] \\ &\simeq - \sum_k \frac{Y_{ik}^\nu Y_{jk}^\nu}{16\pi^2} \left[ \frac{m_{\eta_R}^2}{M_k} \ln\left(\frac{m_{\eta_R}^0}{M_k}\right)^2 \right. \\ &\quad \left. - \frac{m_{\eta_I}^2}{M_k} \ln\left(\frac{m_{\eta_I}^0}{M_k}\right)^2 \right] \quad \text{for } m_{\eta_R}^0, m_{\eta_I}^0 \ll M_k. \end{aligned} \quad (32)$$

Since  $(\mathcal{M}_\nu)_{ij}$  are of order  $10^{-1}$  eV and  $m_{\eta_R}^2 - m_{\eta_I}^2 = \lambda_5 v^2$ , we need  $\sum_k Y_{ik}^\nu Y_{jk}^\nu \lesssim O(10^{-9})$  for  $|\lambda_5| \gtrsim O(0.1)$ . Note, however, that this does not automatically imply that  $\sum_{i,k}^3 |Y_{ik}^\nu|^2 \lesssim O(10^{-9})$ ; and in fact, it could be much larger if we assume a specific flavor structure of  $Y_{jk}^\nu$ . If there exists another source for the neutrino mass matrix, we have to add it to Eq. (32).

### A. Relic abundance of dark matter

Now we come to the relic abundance of DM. Under the assumption about the mass relations [Eq. (26)], we have to consider the following annihilation processes:<sup>5</sup>

$$\bullet \eta_R^0 \eta_R^0 \leftrightarrow \text{SMs}, \quad \bullet \phi \phi \leftrightarrow \text{SMs} \quad (\text{Standard annihilation}), \quad (33)$$

$$\bullet \eta_R^0 \eta_R^0 \leftrightarrow \phi \phi, \quad \bullet \chi \chi \leftrightarrow \phi \phi \quad (\text{Conversion}), \quad (34)$$

$$\bullet \eta_R^0 \chi \leftrightarrow \phi \nu_L, \quad \bullet \chi \phi \leftrightarrow \eta_R^0 \nu_L, \quad \bullet \phi \eta_R^0 \leftrightarrow \chi \nu_L \quad (\text{Semiannihilation}). \quad (35)$$

We have yet not specified the relative sizes of  $m_\chi$  and  $m_\phi$ . If  $\chi$  is lighter than  $\phi$ , the conversion of  $\chi$  into  $\phi$  is kinematically forbidden, and the semiannihilation in Fig. 6 is the only kinematically allowed annihilation for  $\chi$ . So, we will consider below only the case  $m_\chi > m_\phi$ . First, we consider a benchmark set of the input parameter values:

<sup>5</sup>We neglect the coannihilations, such as that of  $\eta_R^0$  with  $\eta_I^0$  and  $\eta^\pm$  below.

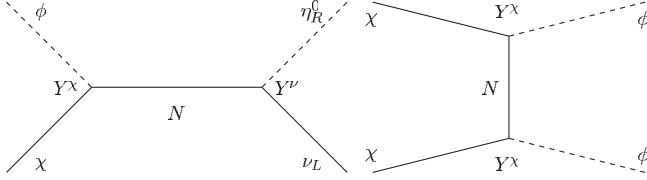


FIG. 6. Semiannihilation (left) and conversion (right).

$$\begin{aligned}
m_{\eta_R^0} &= 200 \text{ GeV}, & m_\chi &= 190 \text{ GeV}, \\
m_\phi &= 180 \text{ GeV}, & m_{\eta^\pm} = m_{\eta_I^0} &= 210 \text{ GeV}, \\
m_h &= 125 \text{ GeV}, & M_1 = M_2 = M_3 &= 1000 \text{ GeV}, \\
\lambda_3 &= -0.065, & \lambda_7 = 0.1, & \lambda_8 = 0.1, \\
\lambda_L &= -0.2, & \sum_{k=1}^3 |Y_k^\chi|^2 &= 3(0.7)^2, \\
& & \sum_{i,k=1}^3 |Y_{ik}^\nu|^2 &= 9(0.01)^2.
\end{aligned} \tag{36}$$

With this choice of the parameter values, we obtain

$$\begin{aligned}
\langle \sigma(\eta_R^0 \eta_R^0; \text{SMs})v \rangle &= 45.66 - 38.21/x, \\
\langle \sigma(\phi\phi; \text{SMs})v \rangle &= 5.93 - 1.92/x, \\
\langle \sigma(\eta_R^0 \eta_R^0; \phi\phi)v \rangle &= 0.46 + 0.29/x, \\
\langle \sigma(\chi\chi; \phi\phi)v \rangle &= 0 + 77.18/x, \\
\langle \sigma(\chi\eta_R^0; \phi\nu_L)v \rangle &= 0.02 + 0.01/x, \\
\langle \sigma(\eta_R^0\phi; \chi\nu_L)v \rangle &= 0.07 + 0.02/x, \\
\langle \sigma(\chi\phi; \eta_R^0\nu_L)v \rangle &= 0.07 + 0.04/x,
\end{aligned} \tag{37}$$

in units of  $10^{-9} \text{ GeV}^{-2}$ , and

$$\begin{aligned}
\Omega_T h^2 &= 0.1094, & \Omega_\eta h^2 &= 0.0062, \\
\Omega_\chi h^2 &= 0.0511, & \Omega_\phi h^2 &= 0.0521,
\end{aligned} \tag{38}$$

where  $x = (1/m_{\eta_R^0} + 1/m_\chi + 1/m_\phi)^{-1}/T = \mu/T$ . As we see from Fig. 6, the size of the semiannihilation and conversion is controlled by  $Y_k^\chi$ . In Fig. 7, we show the  $Y^\chi$  dependence of the individual abundances, where we have varied  $\sum_k |Y_k^\chi|^2$ , and  $Y^\chi/Y_{\text{ref}}^\chi$  stands for  $(\sum_k |Y_k^\chi|^2/3(0.7)^2)^{1/2}$ . If  $Y^\chi/Y_{\text{ref}}^\chi \ll 1$ , the conversion of  $\chi$  and the semiannihilations  $\chi\phi \rightarrow \eta_R^0\nu_L$ ,  $\chi\eta_R^0 \rightarrow \phi\nu_L$  become small, such that  $\Omega_\chi h^2$ , in particular, increases.

## B. Imposing constraints

To be more realistic, we have to impose constraints from direct detection, collider experiments, and perturbativity,  $|\lambda_i|, |Y_{ij}^\nu|, |Y_i^\chi| < 1$ , in addition to Eqs. (27)–(31), which

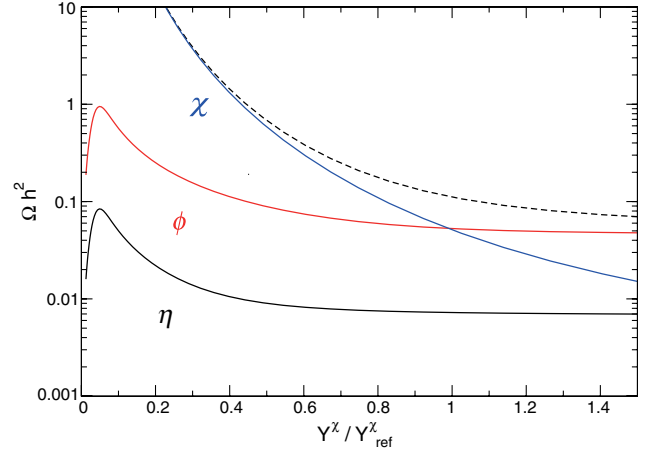


FIG. 7 (color online).  $Y^\chi$  dependence of the relic abundances,  $\Omega_T h^2$  (dashed curve),  $\Omega_\eta h^2$  (black curve),  $\Omega_\chi h^2$  [blue (light gray) curve],  $\Omega_\phi h^2$  [red (gray) curve], where  $Y^\chi$  controls the size of the semiannihilation and conversion shown in Fig. 6. The input parameter values are given in Eq. (36).

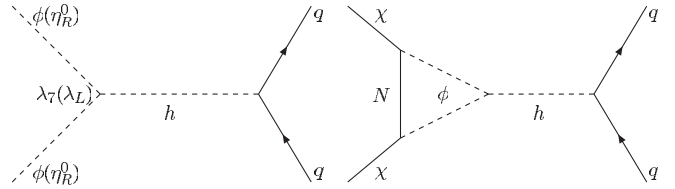


FIG. 8. Tree (left) and one-loop (right) level interactions with the quarks.

we shall do next. The DM particles  $\phi$  and  $\eta_R^0$  have tree-level interactions to the quarks, which are shown in Fig. 8.<sup>6</sup> In the following discussions, we ignore the one-loop contributions such as the right diagram in Fig. 8.<sup>7</sup> The spin-independent elastic cross section off the nucleon  $\sigma(\phi(\eta_R^0))$  is given by [41]

$$\sigma(\phi(\eta_R^0)) = \frac{1}{4\pi} \left( \frac{\lambda_{7(L)} \hat{f} m_N}{m_{\phi(\eta_R^0)} m_h^2} \right)^2 \left( \frac{m_N m_{\phi(\eta_R^0)}}{m_N + m_{\phi(\eta_R^0)}} \right)^2, \tag{39}$$

where  $m_N$  is the nucleon mass, and  $\hat{f} \sim 0.3$  stems from the nucleonic matrix element [61]. The cross sections have to satisfy

$$\left( \frac{\sigma(\phi)}{\sigma_{\text{UB}}(m_\phi)} \right) \left( \frac{\Omega_\phi h^2}{0.112} \right) + \left( \frac{\sigma(\eta_R^0)}{\sigma_{\text{UB}}(m_{\eta_R^0})} \right) \left( \frac{\Omega_\eta h^2}{0.112} \right) \leq 1, \tag{40}$$

where  $\sigma_{\text{UB}}(m)$  is the current experimental limit on the cross section for the DM mass  $m$ .

<sup>6</sup>Direct detection of two DM particles has been discussed, for instance, in Refs. [9,18,19,22]. LHC signals of  $\eta$  dark matter have been discussed in Refs. [41,57,58]. See also Refs. [12,19].

<sup>7</sup>There exist also one-loop corrections to  $\eta_R^0 q \rightarrow \eta_R^0 q$  [59]. See also Ref. [60].

In the absence of  $\chi$  and  $\phi$ , the lower-mass region  $60 \text{ GeV} \leq m_{\eta_R^0} \leq 80 \text{ GeV}$  is consistent with all the experimental constraints [43,57].<sup>8</sup> But the elastic cross section  $\sigma(\eta_R^0) \simeq 7.9 \times 10^{-45} (\lambda_L/0.05)^2 (60 \text{ GeV}/m_{\eta_R^0})^2 \text{ cm}^2$  with  $\lambda_L \geq 0.05$  in this mass range may exceed the upper bound of the XENON100 result [63],<sup>9</sup>  $7.0 \times 10^{-45} \text{ cm}^2$  for the DM mass 50 GeV at a 90% C.L. The higher-mass region, i.e.,  $m_{\eta_R^0} \geq 500 \text{ GeV}$  with  $\sigma(\eta_R^0) \simeq 4.6 \times 10^{-46} (\lambda_L/0.1)^2 (500 \text{ GeV}/m_{\eta_R^0})^2 \text{ cm}^2$ , will be significant for next-generation experiments such as SuperCDMS [70], XENON1T [71] or XMASS [72].

The presence of  $\chi$  and  $\phi$  changes the situation. Firstly, the separation of two allowed regions of  $m_{\eta_R^0}$  disappears: As far as the relic abundance is concerned,  $m_{\eta_R^0}$  is allowed between 80 and 500 GeV too, as we have seen, because  $\chi$  and  $\phi$  also contribute to the relic abundance. Secondly, the parameter space becomes considerably larger. To see how the allowed parameter space of the model without  $\chi$  and  $\phi$  changes, we consider a set of  $(\delta_1 = m_{\eta^\pm} - m_{\eta_R^0}, \delta_2 = m_{\eta_1^0} - m_{\eta_R^0})$ , for which the allowed parameter space without  $\chi$  and  $\phi$  is very small. For  $(\delta_1 = 10, \delta_2 = 10) \text{ GeV}$ , for instance, there is no allowed range of  $m_{\eta_R^0} \leq 500 \text{ GeV}$  [43]; the low-mass range of  $m_{\eta_R^0}$ , for which the relic abundance  $\Omega_\eta h^2$  is consistent, does not satisfy the LEP constraint. Below we show how this situation changes in the presence of  $\chi$  and  $\phi$ . The LEP constraint implies that the region satisfying  $m_{\eta_R^0} \leq 80 \text{ GeV}$  and  $m_{\eta_1^0} \leq 100 \text{ GeV}$  with  $\delta_2 \geq 8 \text{ GeV}$  is excluded [43]. Therefore, for  $(\delta_1 = 10, \delta_2 = 10) \text{ GeV}$ , we have to consider only  $m_{\eta_R^0} > 80 \text{ GeV}$ . Further, to suppress the parameter space, we assume that  $m_\chi = m_{\eta_R^0} - 10 \text{ GeV}$ ,  $m_\phi = m_{\eta_R^0} - 20 \text{ GeV}$ , and  $M_k = 1000 \text{ GeV}$ , and we scan  $m_{\eta_R^0}$  from 80 to 500 GeV.

Figure 9 shows the allowed area in the  $\lambda_L(\lambda_7)-m_{\eta_R^0}$  plane, where all the constraints are taken into account. The allowed mass range for  $m_{\eta_R^0}$  is extended as expected. The reason that there are no allowed points around  $m_{\eta_R^0} \simeq 100 \text{ GeV}$  is the following: Since we keep the mass difference fixed, we have  $m_\phi = m_{\eta_R^0} - 20 \simeq 80 \text{ GeV}$  there. This is the threshold regime for the process  $\phi\phi \rightarrow W^+W^-$ . So, for  $m_{\eta_R^0}$  just below 100 GeV, the annihilation cross section for  $\phi$  is small because of small  $\lambda_7$  in this range of  $m_\phi$ , and therefore the relic abundance  $\Omega_\phi h^2$  exceeds 0.12. We see that  $m_{\eta_R^0} = 80 \text{ GeV}$  is allowed, on the other hand. This allowed area exists, though  $\lambda_7$  is small, because around  $m_\phi = 62 \text{ GeV}$ , the  $s$ -channel annihilation of  $\phi$  becomes resonant due to  $m_h = 125 \text{ GeV}$ . For  $m_{\eta_R^0}$  just above 100 GeV, the annihilation cross section for  $\phi$  is large

<sup>8</sup>There exists a marginal possibility to expand slightly this upper bound [62].

<sup>9</sup>See also Refs. [64–69].

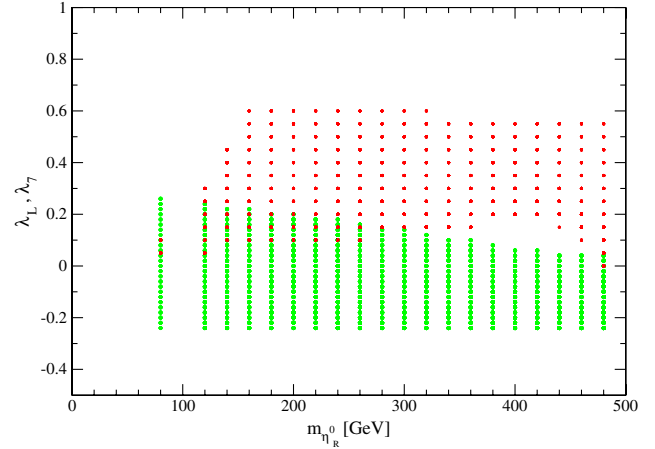


FIG. 9 (color online). The allowed regime in the  $\lambda_L(\lambda_7)-m_{\eta_R^0}$  plane for  $(\delta_1 = 10, \delta_2 = 10) \text{ GeV}$  with  $m_\chi = m_{\eta_R^0} - 10 \text{ GeV}$ ,  $m_\phi = m_{\eta_R^0} - 20 \text{ GeV}$  and  $M_k = 1000 \text{ GeV}$ . The green (light gray) and red (dark gray) points are for  $\lambda_L$  and  $\lambda_7$ , respectively.

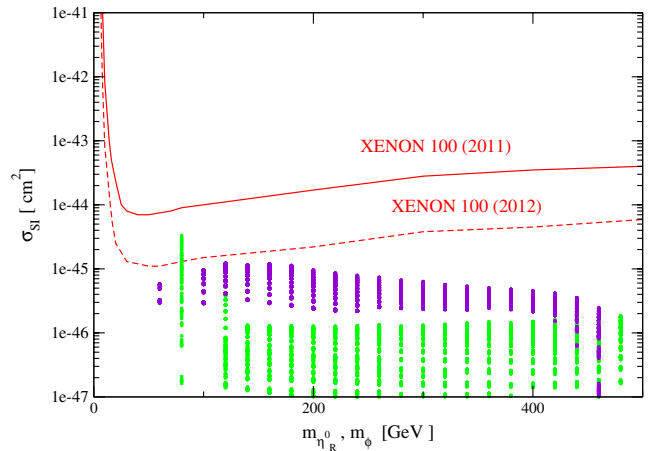


FIG. 10 (color online). The spin-independent cross section off the nucleon is plotted as a function of the DM mass. The green (light gray) and violet (dark gray) areas are for  $\eta$  and  $\phi$  DM's, respectively, where we have used  $(\delta_1 = 10, \delta_2 = 10) \text{ GeV}$  with  $m_\chi = m_{\eta_R^0} - 10 \text{ GeV}$ ,  $m_\phi = m_{\eta_R^0} - 20 \text{ GeV}$  and  $M_k = 1000 \text{ GeV}$ .

because the channel to  $W^+W^-$  is now open, so that  $\Omega_\phi h^2$  cannot supplement the anyhow small  $\Omega_\eta h^2$ .

If we suppress the constraint from direct detection, we have a prediction on direct detection. Figure 10 shows the spin-independent cross section off the nucleon versus the DM mass; the green (light gray) does so for the  $\eta$  DM, and violet (dark gray) area for the  $\phi$  DM. We see that the spin-independent cross sections not only are consistent with the current bound of XENON100 [63], but also are within the accessible range of future experiments.

### C. Indirect detection

If DM annihilates sufficiently into SM particles, the resulting cosmic rays may be observable. These are

indirect signals of DM, and in fact excesses in  $e^+$  [73–76] and in  $\gamma$  [77–80] have recently been reported. Indirect detection of DM has been studied within the framework of a two-component DM system in Refs. [8,10,13–15,18,26,27], and also within the inert Higgs model in Refs. [42,81–83]. As we see from the semiannihilation diagram in Fig. 6, the process produces only a left-handed neutrino as the SM particle. Therefore, we are particularly interested in the neutrinos from the annihilation of captured DM in the Sun [44–53] (see Refs. [4,5] for a review, and Refs. [83,84] for the case of the inert Higgs model), because (i) the semiannihilation produces a monochromatic neutrino ( $E_\nu \simeq m_{\eta_R^0} + m_\phi - m_\chi$ , for instance) in addition to those with  $E_\nu \simeq m_{\eta_R^0}$  along with the continuum spectrum, (ii) these neutrinos can be observed at neutrino telescopes [85–87], and (iii) the evolution equations of the DM numbers in the Sun, which describe approaching equilibrium between the capture and annihilation (including conversion and semiannihilation) rates of DM, are coupled now.

We denote the number of DM particles  $\eta$ ,  $\chi$  and  $\phi$  in the Sun by  $N_i$ , with  $i = \eta$ ,  $\chi$  and  $\phi$ , respectively. Then the change of  $N_i$  with respect to time  $t$  is given by

$$\begin{aligned} \dot{N}_\eta = & C_\eta - C_A(\eta\eta \leftrightarrow \text{SM})N_\eta^2 - C_A(\eta\eta \leftrightarrow \phi\phi)N_\eta^2 \\ & - C_A(\eta\chi \leftrightarrow \phi\nu_L)N_\eta N_\chi - C_A(\eta\phi \leftrightarrow \chi\nu_L)N_\eta N_\phi \\ & + C_A(\phi\chi \leftrightarrow \eta\nu_L)N_\chi N_\phi, \end{aligned} \quad (41)$$

$$\begin{aligned} \dot{N}_\chi = & C_\chi - C_A(\chi\chi \leftrightarrow \phi\phi)N_\chi^2 - C_A(\eta\chi \leftrightarrow \phi\nu_L)N_\eta N_\chi \\ & + C_A(\eta\phi \leftrightarrow \chi\nu_L)N_\eta N_\phi - C_A(\phi\chi \leftrightarrow \eta\nu_L)N_\chi N_\phi, \end{aligned} \quad (42)$$

$$\begin{aligned} \dot{N}_\phi = & C_\phi - C_A(\phi\phi \leftrightarrow \text{SM})N_\phi^2 + C_A(\eta\eta \leftrightarrow \phi\phi)N_\eta^2 \\ & + C_A(\chi\chi \leftrightarrow \phi\phi)N_\chi^2 + C_A(\eta\chi \leftrightarrow \phi\nu_L)N_\eta N_\chi \\ & - C_A(\eta\phi \leftrightarrow \chi\nu_L)N_\eta N_\phi - C_A(\phi\chi \leftrightarrow \eta\nu_L)N_\chi N_\phi, \end{aligned} \quad (43)$$

where the  $C_i$ 's are the capture rates in the Sun, and the  $C_A$ 's are proportional to the annihilation cross sections times the relative DM velocity per volume in the limit  $v \rightarrow 0$ :

$$\begin{aligned} C_{\phi(\eta)} \simeq & 1.4 \times 10^{20} f(m_{\phi(\eta_R^0)}) \left(\frac{\hat{f}}{0.3}\right)^2 \left(\frac{\lambda_{7(L)}}{0.1}\right)^2 \left[\frac{m_h}{125 \text{ GeV}}\right]^{-4} \\ & \times \left(\frac{200 \text{ GeV}}{m_{\phi(\eta_R^0)}}\right)^2 \left(\frac{\Omega_{\phi(\eta)} h^2}{0.112}\right) \text{s}^{-1}, \quad C_\chi = 0, \end{aligned} \quad (44)$$

where the function  $f(m_{\phi(\eta_R^0)})$  depends on the form factor of the nucleus, elemental abundance, kinematic suppression of the capture rate, etc., varying from  $O(1)$  to  $O(0.01)$  depending on the DM mass [50,51]. The annihilation rates,  $C_A$ , can be calculated from [48]

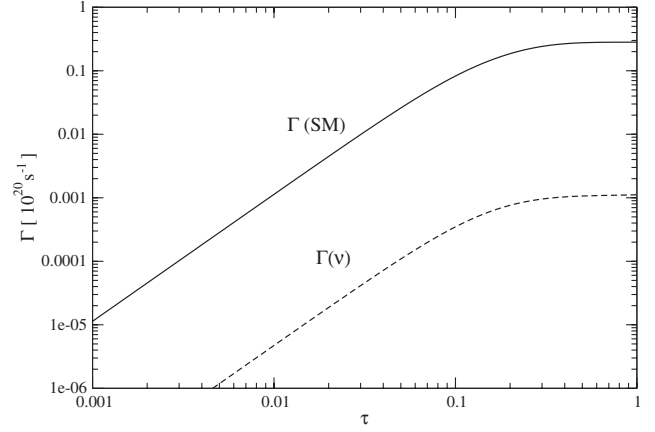


FIG. 11. The time evolution of the annihilation rates  $\Gamma(\text{SM})$  and  $\Gamma(\nu)$ , where  $\tau = t/t_0$ , and the input parameter values are those given in Eq. (36).

$$C_A(ij \leftrightarrow \bullet) = \frac{\langle \sigma(ij; \bullet)v \rangle}{V_{ij}}, \quad (45)$$

$$V_{ij} = 5.7 \times 10^{27} \left(\frac{100 \text{ GeV}}{\mu_{ij}}\right)^{3/2} \text{ cm}^3,$$

with  $\mu_{ij} = 2m_i m_j / (m_i + m_j)$  in the limit  $v \rightarrow 0$ .

There are fixed points of the evolution equations which correspond to equilibrium. Since at the time of the Sun's birth the numbers  $N_i$  were zero, the  $N_i$ 's increase with time and approach the fixed-point values, i.e., equilibrium, at which point  $N_i$  assumes its maximal value. So, the question is whether the age of the Sun,  $t_0 \simeq 4.5 \times 10^9$  years, is old enough for  $N_i$  to reach equilibrium. We see from the evolution equations that the fixed-point values are roughly proportional to  $(C_i/C_A)^{1/2}$ , implying that we need large capture rates  $C_i$  to obtain large  $N_i(t_0)$ . The annihilation, conversion and semiannihilation rates at  $t = t_0$  are given by

$$\Gamma(ij; \bullet) = d_{ij} C_A(ij \leftrightarrow \bullet) N_i(t_0) N_j(t_0), \quad (46)$$

where  $d_{ii} = 1/2$  and  $d_{ij} = 1$  for  $i \neq j$ . The observation rate of the neutrinos,  $\Gamma_{\text{detect}}$ , is proportional to  $\Gamma(ij; \bullet)$ . As a benchmark, we use the same set of input parameter values as in Eq. (36). In Fig. 11, we show the time evolution of<sup>10</sup>

$$\Gamma(\text{SM}) = C_A(\eta\eta \leftrightarrow \text{SM})N_\eta^2/2 + C_A(\phi\phi \leftrightarrow \text{SM})N_\phi^2/2, \quad (47)$$

<sup>10</sup>For the monochromatic neutrinos, i.e.,  $\Gamma(\nu)$ , we have added all the semiannihilations, because for the mass values given in Eq. (36), the neutrino energies are all close to 200 GeV. Moreover, the first term in the rhs of Eq. (48) (which counts neutrinos of  $m_{\eta_R^0} + m_\phi - m_\chi = 190 \text{ GeV}$ ) is a dominant contribution with about 95%.

$$\Gamma(\nu) = C_A(\eta\phi \leftrightarrow \chi\nu)N_\eta N_\phi + C_A(\eta\chi \leftrightarrow \phi\nu)N_\eta N_\chi + C_A(\chi\phi \leftrightarrow \eta\nu)N_\chi N_\phi, \quad (48)$$

$$\Gamma(\nu\nu) = C_A(\eta\eta \leftrightarrow \nu\nu)N_\eta^2/2, \quad (49)$$

scaled to  $10^{20} \text{ s}^{-1}$ , as a function of  $\tau = t/t_\odot$ . As we see from Fig. 11, the rates seem to be saturated:  $\Gamma(\text{SM})$  is in fact saturated, but  $\Gamma(\nu)$  does not reach its fixed-point value of  $0.002 \times 10^{20} \text{ s}^{-1}$  at  $\tau = t/t_\odot = 1$ . The saturated value of  $\Gamma(\text{SM})$  is  $0.28 \times 10^{20} \text{ s}^{-1}$  for the input parameters of Eq. (36), which is consistent with the upper limit of  $\sim 2.73 \times 10^{21} \text{ s}^{-1}$  for  $m_{\text{DM}} = 250 \text{ GeV}$  of the AMANDA-II/IceCube neutrino telescope [85]. As for the monochromatic neutrinos, we obtain  $\Gamma(\nu) = 1.1 \times 10^{-3} \times 10^{20} \text{ s}^{-1}$  and  $\Gamma(\nu\nu) = 1.3 \times 10^{-7} \times 10^{20} \text{ s}^{-1}$ . To estimate the detection rate  $\Gamma_{\text{detect}}$ , we use the formula [88]

$$\Gamma_{\text{detect}} = AP(E_\nu)\Gamma_{\text{inc}}, \quad (50)$$

where  $A$  is the detector area facing the incident beam,  $P(E_\nu)$  is the probability for detection as a function of the neutrino energy  $E_\nu$ , and  $\Gamma_{\text{inc}} = \Gamma/4\pi R_\odot^2$  is the incoming neutrino flux—i.e., the number of neutrinos per unit area per second on the Earth (where  $R_\odot$  is the distance to the Sun  $\simeq 1.5 \times 10^8 \text{ km}$ ).<sup>11</sup> The probability  $P(E_\nu)$  may be approximated as the ratio of the effective detector length  $L$  to the mean free path of the neutrinos in the detector. For the neutrinos (antineutrinos), one finds  $P(E_{\nu(\bar{\nu})}) \simeq 2.0(1.0) \times 10^{-11}(L/\text{km})(E_{\nu(\bar{\nu})}/\text{GeV})$ , arriving at

$$\Gamma_{\text{detect}} \simeq 2.2(1.1) \times 10^{-21} \left(\frac{A}{\text{km}^2}\right) \left(\frac{L}{\text{km}}\right) \left(\frac{E_{\nu(\bar{\nu})}}{\text{GeV}}\right) \left(\frac{\Gamma}{\text{s}^{-1}}\right) \text{yr}^{-1}, \quad (51)$$

which implies that, for the input parameters of Eq. (36), 0.05 events of monochromatic neutrinos with  $\sim 200 \text{ GeV}$  per year may be detected at IceCube [85], where we have used  $A = 1 \text{ km}^2$ ,  $L = 1 \text{ km}$ .

A total of 0.05 events per year may be too small to be realistic. However, we would like to note that we have studied only one point in the whole parameter space. It will be our future program to implement the sophisticated method of Ref. [89] and to survey the whole parameter space. How to observe the monochromatic neutrinos at

<sup>11</sup>A sophisticated method to compute the observation rates at IceCube was recently developed in Ref. [89].

neutrino telescopes should also be addressed [90]. Finally, we would like to note that if at least one of the fermionic DM particles in a multicomponent DM system has odd parity of the discrete lepton number, then a monochromatic left-handed neutrino, which is also odd, can be produced together with this fermionic DM in a semiannihilation of DM particles.

#### IV. CONCLUSION

We have considered the conversion and semiannihilation of DM in a multicomponent DM system. We have found in fictive models that these nonstandard DM annihilation processes can influence the relic abundance of DM a lot, which has been recently found for two-component DM systems in Refs. [17,22,23].

As a concrete three-component DM system, we have considered a radiative seesaw model of Ref. [32], which is extended to include an extra Majorana fermion  $\chi$  and an extra real scalar boson  $\phi$ . The DM stabilizing symmetry is promoted to  $Z_2 \times Z'_2$ , and we have assumed that  $\eta_R^0$  (the  $CP$ -even neutral component of the inert Higgs  $SU(2)_L$  doublet),  $\chi$  and  $\phi$  are DM. We have shown that the previously found separation [41–43] of the allowed parameter space in the low- and high-mass regions for  $\eta_R^0$  disappears in the presence of  $\chi$  and  $\phi$ .

Finally, we have discussed neutrinos coming from the annihilations of the captured DM in the Sun. The evolution equations of the DM numbers in the Sun, which describe approaching equilibrium between the capture and annihilation (including conversion and semiannihilation) rates of DM, are coupled in a multicomponent DM system. Due to the semiannihilations of DM, monochromatic neutrinos are radiated, and the observation rates of neutrinos have been estimated. Observations of high-energy monochromatic neutrinos from the Sun may indicate a multicomponent DM system.

#### ACKNOWLEDGMENTS

The work of M.D. is supported by the International Max Planck Research School for Precision Tests of Fundamental Symmetries. The work of M. A. is supported in part by the Grant-in-Aid for Scientific Research for Young Scientists (B) (Grant No. 22740137), and J. K. is partially supported by the Grant-in-Aid for Scientific Research (C) from the Japan Society for Promotion of Science (Grant No. 22540271). M.D. thanks the Institute for Theoretical Physics at Kanazawa University for very kind hospitality.

- [1] A. G. Riess *et al.* (Supernova Search Team Collaboration), *Astron. J.* **116**, 1009 (1998).
- [2] K. N. Abazajian *et al.* (SDSS Collaboration), *Astrophys. J. Suppl. Ser.* **182**, 543 (2009).
- [3] E. Komatsu *et al.* (WMAP Collaboration), *Astrophys. J. Suppl. Ser.* **192**, 18 (2011).
- [4] G. Jungman, M. Kamionkowski, and K. Griest, *Phys. Rep.* **267**, 195 (1996).
- [5] G. Bertone, D. Hooper, and J. Silk, *Phys. Rep.* **405**, 279 (2005); *Particle Dark Matter: Observations, Models and Searches*, edited by G. Bertone (Cambridge University Press, Cambridge, England, 2010).
- [6] M. Cirelli, [arXiv:1202.1454](https://arxiv.org/abs/1202.1454).
- [7] Z. G. Berezhiani and M. Y. Khlopov, *Yad. Fiz.* **52**, 96 (1990) [*Sov. J. Nucl. Phys.* **52**, 60 (1990)]; *Z. Phys. C* **49**, 73 (1991).
- [8] C. Boehm, P. Fayet, and J. Silk, *Phys. Rev. D* **69**, 101302 (2004).
- [9] T. Hur, H.-S. Lee, and S. Nasri, *Phys. Rev. D* **77**, 015008 (2008).
- [10] Q. H. Cao, E. Ma, J. Wudka, and C. P. Yuan, [arXiv:0711.3881](https://arxiv.org/abs/0711.3881).
- [11] J. L. Feng and J. Kumar, *Phys. Rev. Lett.* **101**, 231301 (2008).
- [12] H. S. Cheon, S. K. Kang, and C. S. Kim, *Phys. Lett. B* **675**, 203 (2009); **698**, 324(E) (2011).
- [13] J.-H. Huh, J. E. Kim, and B. Kyae, *Phys. Rev. D* **79**, 063529 (2009).
- [14] M. Fairbairn and J. Zupan, *J. Cosmol. Astropart. Phys.* **07** (2009) 001.
- [15] K. M. Zurek, *Phys. Rev. D* **79**, 115002 (2009).
- [16] D. E. Morrissey, D. Poland, and K. M. Zurek, *J. High Energy Phys.* **07** (2009) 050.
- [17] F. D'Eramo and J. Thaler, *J. High Energy Phys.* **06** (2010) 109.
- [18] D. Feldman, Z. Liu, P. Nath, and G. Peim, *Phys. Rev. D* **81**, 095017 (2010).
- [19] B. Batell, *Phys. Rev. D* **83**, 035006 (2011).
- [20] Z.-P. Liu, Y.-L. Wu, and Y.-F. Zhou, *Eur. Phys. J. C* **71**, 1749 (2011).
- [21] K. R. Dienes and B. Thomas, *Phys. Rev. D* **85**, 083523 (2012); **85**, 083524 (2012); K. R. Dienes, S. Su, and B. Thomas, [arXiv:1204.4183](https://arxiv.org/abs/1204.4183) [*Phys. Rev. D* (to be published)].
- [22] G. Belanger and J.-C. Park, *J. Cosmol. Astropart. Phys.* **03** (2012) 038.
- [23] G. Belanger, K. Kannike, A. Pukhov, and M. Raidal, *J. Cosmol. Astropart. Phys.* **04** (2012) 010.
- [24] I. P. Ivanov and V. Keus, *Phys. Rev. D* **86**, 016004 (2012).
- [25] E. Ma, *Ann. Fond. Louis de Broglie* **31**, 285 (2006); *Mod. Phys. Lett. A* **23**, 721 (2008).
- [26] H. Fukuoka, J. Kubo, and D. Suematsu, *Phys. Lett. B* **678**, 401 (2009).
- [27] H. Fukuoka, D. Suematsu, and T. Toma, *J. Cosmol. Astropart. Phys.* **07** (2011) 001.
- [28] D. Suematsu and T. Toma, *Nucl. Phys.* **B847**, 567 (2011).
- [29] M. Aoki, J. Kubo, T. Okawa, and H. Takano, *Phys. Lett. B* **707**, 107 (2012).
- [30] E. Ma, *Phys. Lett. B* **662**, 49 (2008).
- [31] K. Agashe, D. Kim, M. Toharia, and D. G. E. Walker, *Phys. Rev. D* **82**, 015007 (2010).
- [32] E. Ma, *Phys. Rev. D* **73**, 077301 (2006).
- [33] K. Griest, *Phys. Rev. D* **38**, 2357 (1988); **39**, 3802(E) (1989).
- [34] M. Srednicki, R. Watkins, and K. A. Olive, *Nucl. Phys.* **B310**, 693 (1988).
- [35] K. Griest, M. Kamionkowski, and M. S. Turner, *Phys. Rev. D* **41**, 3565 (1990).
- [36] E. W. Kolb and M. S. Turner, *Front. Phys.* **69**, 1 (1990).
- [37] P. Gondolo and G. Gelmini, *Nucl. Phys.* **B360**, 145 (1991).
- [38] M. Drees and M. M. Nojiri, *Phys. Rev. D* **47**, 376 (1993).
- [39] K. Griest and D. Seckel, *Phys. Rev. D* **43**, 3191 (1991).
- [40] J. R. Ellis, T. Falk, and K. A. Olive, *Phys. Lett. B* **444**, 367 (1998); J. R. Ellis, T. Falk, K. A. Olive, and M. Srednicki, *Astropart. Phys.* **13**, 181 (2000); **15**, 413(E) (2001).
- [41] R. Barbieri, L. J. Hall, and V. S. Rychkov, *Phys. Rev. D* **74**, 015007 (2006).
- [42] L. Lopez-Honorez, E. Nezri, J. F. Oliver, and M. H. G. Tytgat, *J. Cosmol. Astropart. Phys.* **02** (2007) 028.
- [43] E. M. Dolle and S. Su, *Phys. Rev. D* **80**, 055012 (2009).
- [44] J. Silk, K. A. Olive, and M. Srednicki, *Phys. Rev. Lett.* **55**, 257 (1985).
- [45] L. M. Krauss, M. Srednicki, and F. Wilczek, *Phys. Rev. D* **33**, 2079 (1986).
- [46] K. Freese, *Phys. Lett.* **167B**, 295 (1986).
- [47] T. K. Gaisser, G. Steigman, and S. Tilav, *Phys. Rev. D* **34**, 2206 (1986).
- [48] K. Griest and D. Seckel, *Nucl. Phys.* **B283**, 681 (1987); **B296**, 1034(E) (1988).
- [49] S. Ritz and D. Seckel, *Nucl. Phys.* **B304**, 877 (1988).
- [50] M. Kamionkowski, *Phys. Rev. D* **44**, 3021 (1991).
- [51] M. Kamionkowski, K. Griest, G. Jungman, and B. Sadoulet, *Phys. Rev. Lett.* **74**, 5174 (1995).
- [52] H.-C. Cheng, J. L. Feng, and K. T. Matchev, *Phys. Rev. Lett.* **89**, 211301 (2002).
- [53] D. Hooper and G. D. Kribs, *Phys. Rev. D* **67**, 055003 (2003).
- [54] E. Ma and M. Raidal, *Phys. Rev. Lett.* **87**, 011802 (2001); **87**, 159901(E) (2001).
- [55] K. Hayasaka, [arXiv:1010.3746](https://arxiv.org/abs/1010.3746).
- [56] K. Nakamura *et al.* (Particle Data Group Collaboration), *J. Phys. G* **37**, 075021 (2010, and 2011 partial update for the 2012 edition).
- [57] M. Gustafsson, S. Rydbeck, L. Lopez-Honorez, and E. Lundstrom, [arXiv:1206.6316](https://arxiv.org/abs/1206.6316) [*Phys. Rev. D* (to be published)].
- [58] E. Dolle, X. Miao, S. Su, and B. Thomas, *Phys. Rev. D* **81**, 035003 (2010).
- [59] M. Cirelli, N. Fornengo, and A. Strumia, *Nucl. Phys.* **B753**, 178 (2006).
- [60] D. Schmidt, T. Schwetz, and T. Toma, *Phys. Rev. D* **85**, 073009 (2012).
- [61] J. R. Ellis, A. Ferstl, and K. A. Olive, *Phys. Lett. B* **481**, 304 (2000).
- [62] L. L. Honorez and C. E. Yaguna, *J. Cosmol. Astropart. Phys.* **01** (2011) 002.
- [63] E. Aprile *et al.* (XENON100 Collaboration), *Phys. Rev. Lett.* **107**, 131302 (2011).

- [64] G. Angloher, M. Bauer, I. Bavykina, A. Bento, A. Brown, C. Bucci, C. Ciemniak, C. Coppi, G. Deuter, F. von Feilitzsch *et al.*, *Astropart. Phys.* **31**, 270 (2009).
- [65] V.N. Lebedenko, H.M. Araujo, E.J. Barnes, A. Bewick, R. Cashmore, V. Chepel, A. Currie, D. Davidge *et al.*, *Phys. Rev. D* **80**, 052010 (2009).
- [66] Z. Ahmed *et al.* (CDMS-II Collaboration), *Science* **327**, 1619 (2010).
- [67] C.E. Aalseth *et al.* (CoGeNT Collaboration), *Phys. Rev. Lett.* **106**, 131301 (2011).
- [68] R. Bernabei *et al.* (DAMA and LIBRA Collaborations), *Eur. Phys. J. C* **67**, 39 (2010).
- [69] S. C. Kim, H. Bhang, J. H. Choi, W. G. Kang, B. H. Kim, H. J. Kim, K. W. Kim, S. K. Kim *et al.*, *Phys. Rev. Lett.* **108**, 181301 (2012).
- [70] T. Bruch (CDMS Collaboration), [arXiv:1001.3037](https://arxiv.org/abs/1001.3037).
- [71] M. Selvi (XENON1T Collaboration), Proc. Sci., IDM2010 (2011) 053.
- [72] H. Sekiya, *J. Phys. Conf. Ser.* **308**, 012011 (2011).
- [73] O. Adriani *et al.* (PAMELA Collaboration), *Nature (London)* **458**, 607 (2009).
- [74] S. W. Barwick *et al.* (HEAT Collaboration), *Astrophys. J.* **482**, L191 (1997).
- [75] M. Aguilar *et al.* (AMS-01 Collaboration), *Phys. Lett. B* **646**, 145 (2007).
- [76] M. Ackermann *et al.* (LAT Collaboration), *Phys. Rev. Lett.* **108**, 011103 (2012).
- [77] F. Aharonian *et al.* (HESS Collaboration), *Astron. Astrophys.* **425**, L13 (2004); *Phys. Rev. Lett.* **97**, 221102 (2006); **97**, 249901(E) (2006).
- [78] W. B. Atwood *et al.* (LAT Collaboration), *Astrophys. J.* **697**, 1071 (2009).
- [79] J. Aleksic *et al.* (MAGIC Collaboration), *Astrophys. J.* **710**, 634 (2010).
- [80] V. A. Acciari *et al.* (VERITAS Collaboration), *Astrophys. J.* **720**, 1174 (2010).
- [81] M. Gustafsson, E. Lundstrom, L. Bergstrom, and J. Edsjo, *Phys. Rev. Lett.* **99**, 041301 (2007).
- [82] D. Suematsu, T. Toma, and T. Yoshida, *Phys. Rev. D* **82**, 013012 (2010).
- [83] P. Agrawal, E. M. Dolle, and C. A. Krenke, *Phys. Rev. D* **79**, 015015 (2009).
- [84] S. Andreas, M. H. G. Tytgat, and Q. Swillens, *J. Cosmol. Astropart. Phys.* **04** (2009) 004.
- [85] R. Abbasi *et al.* (IceCube Collaboration), *Phys. Rev. D* **85**, 042002 (2012).
- [86] T. Tanaka *et al.* (Super-Kamiokande Collaboration), *Astrophys. J.* **742**, 78 (2011).
- [87] J. D. Zornoza, [arXiv:1204.5066](https://arxiv.org/abs/1204.5066).
- [88] F. Halzen and S. R. Klein, *Rev. Sci. Instrum.* **81**, 081101 (2010).
- [89] P. Scott *et al.* (IceCube Collaboration), [arXiv:1207.0810](https://arxiv.org/abs/1207.0810).
- [90] A. Esmaili and Y. Farzan, *Phys. Rev. D* **81**, 113010 (2010); *J. Cosmol. Astropart. Phys.* **04** (2011) 007.